Diagnostic Significance of Orbit Shape Analysis and its Application to Improve Machine Fault Detection

Nicolò Bachschmid
Politecnico di Milano
Department of Mechanics
Via La Masa 34, I-20158, Milano, Italy
nicolo.bachschmid@polimi.it

Paolo Pennacchi
Politecnico di Milano
Department of Mechanics
Via La Masa 34, I-20158, Milano, Italy
paolo.pennacchi@polimi.it

Andrea Vania
Politecnico di Milano
Department of Mechanics
Via La Masa 34, I-20158, Milano, Italy
andrea.vania@polimi.it

The full spectrum analysis of rotating machine vibrations is a diagnostic tool that enables the symptoms of some special types of fault to be clearly detected. The Shape and Directivity Index (SDI) of journal filtered orbits is an additional diagnostic parameter whose evaluation can be combined with the full spectrum analysis. The ellipticity of the filtered orbit, as well as the amplitude and the inclination angle of the major axis of the orbit, are parameters whose analysis can provide important diagnostic information. In order to validate the proposed approach, the vibrations of a large turbine–generator unit that was subjected to rotor–to–stator rubs have been analyzed in this paper. The results of this investigation have been used to update the model of the rotor–system that has been used to identify the location and the severity of the fault. In the paper, the improvements in the accuracy of the fault identification provided by the model updating enabled by the SDI analysis are shown.
***Keywords**: Rotating machines, vibrations, fault identification, rubs, condition monitoring.*

Introduction

Often, the identification of faults in rotating machines requires to use model–based techniques. Anyhow, a preliminary fault symptom analysis can provide important diagnostic indications that can be used for more detailed investigations. The full spectrum of the vibration measured is one of the possible tools of analysis (Southwick, 1993, 1994, Lee and Joh, 1994, Lee et al., 1997a, 1997b), which can be integrated by the Shape and Directivity Index (SDI). They allow the symptoms of some types of faults to be clearly detected (Lee and Han, 1998, 1999). The analysis of both orientation and ellipticity of the journal filtered orbits (1X, 2X) can provide significant information about the dynamic stiffness of the bearings, the oil–film geometry, the machine alignment and the presence of sideloads on the rotor. In addition to this, both full spectrum and SDI are useful diagnostic tools because they allow the direction of precession to be evaluated.

Usually, the analysis of the orbit shape is carried out for a limited number of rotating speeds, Ω. Conversely, in this paper, the continuous changes of the shape and directivity index that occur during the rotating speed transients have been considered. The curve of the function SDI(Ω), evaluated using the vibration data measured with the machine in normal condition, can be used as a reference baseline. Significant changes in the actual SDI(Ω) curve, with respect to the reference curve, indicate a fault symptom. Additional information can be obtained with the analysis of the amplitude and the inclination angle of the major axis of the filtered orbits. Also the changes of the current values of these parameters, in comparison with their reference values, can be assumed as a fault symptom. Therefore, the numerous diagnostic information that can be obtained by the onerous analysis of several orbit diagrams can be condensed into a limit number of curves determined by processing transient vibration data. The results provided by the full spectrum and the SDI analysis can be very important because, depending on the type and the severity of the fault, the dynamic stiffness of the bearings can change. Therefore, on the basis of the results of these analyses, the tuning of the model used to identify the fault can be refined.

In order to validate the capabilities of this diagnostic approach, the transient vibrations of a turbine–generator unit that was subjected to light but significant rotor–to–stator rubs have been analyzed. Owing to the heating induced by the rubs, the turbine shaft was affected by a bow whose severity changed during the speed transient. At low rotating speeds, when the amplitude of the shaft bow became noticeable, the dynamic stiffness of some journal bearings was affected by the high levels of the shaft vibrations. This phenomenon must be considered when the machine dynamic behavior is simulated with a linear model both of bearings and rotors.

A model–based identification method, developed by the authors and described in previous papers (Bachschmid et al., 2002), has been used to estimate a suitable set of the equivalent excitations, applied to the turbine shaft, which induce shaft vibrations that are very similar to those caused by the rubs. In the paper, the journal orbits evaluated using the numerical results provided by the simulating model have been compared with those evaluated on the basis of the experimental transient vibrations.

Nomenclature

a = major semi-axis of elliptical orbit
p = complex signal defined by Eq. (2)
r = harmonic component of the complex signal $p(t)$
SDI = Shape and Directivity Index defined by Eq. (1), dimensionless
x = vibration signal
y = vibration signal
$\mathbf{X}_{exp}$ = experimental vibration vector
$\mathbf{X}_{th}$ = simulated vibrations vector

Greek Symbols

ε = residual, fault identification error, dimensionless
φ = inclination angle of the major axis of elliptical filtered orbits
ω = frequency (pulsation), rad/s
Ω = rotating speed, rad/s

Subscripts

d direct part of a complex variable
q quadrature part of a complex variable

Shape and Directivity Index

The diagnostic method used in this paper is based on the analysis of the journal filtered orbits (1X, 2X) determined with a couple of radial and orthogonal (*XY*) vibration probes. The analysis of the filtered orbits is obtained by evaluating the degree of

ellipticity and the inclination angle of the major axis of the orbit with respect to the horizontal axis. The degree of ellipticity of the orbit is provided by the Shape and Directivity Index (SDI) which is defined as (Lee and Han, 1998, 1999):

$$-1 \le \mathrm{SDI} = \frac{\left|r^f\right| - \left|r^b\right|}{\left|r^f\right| + \left|r^b\right|} \le 1 \tag{1}$$

where r^f and r^b are, respectively, the forward and backward harmonic components of the complex harmonic signal $p(t)$ of frequency ω. The real and imaginary parts of the signal $p(t)$ are the real vibration signals, filtered at frequency ω, measured along the shaft in the two orthogonal directions X and Y, respectively. Therefore, the complex signal $p(t)$ can be written in polar form, using the Euler's formula, as:

$$p(t) = x(t) + j \;\; y(t) = p^f(t) + j \;\; p^b(t) = r^f e^{j\omega t} + r^b e^{-j\omega t} \tag{2}$$

By denoting x_d, x_q, y_d and y_q the direct and quadrature parts of the filtered vibration signals $x(t)$ and $y(t)$, respectively, the complex signal $p(t)$ can be rewritten in the following form:

$$\begin{aligned} p(t) = &\frac{1}{2}\left\{(x_d + y_q) + j \;\; (y_d - x_q)\right\} e^{j\omega t} + \\ &+ \frac{1}{2}\left\{(x_d - y_q) + j \;\; (y_d + x_q)\right\} e^{-j\omega t} \end{aligned} \tag{3}$$

The sign of the SDI index determines the directivity of the orbit while the absolute value of the SDI gives the degree of ellipticity. In fact, a positive unity value of the SDI indicates a forward circular motion while a negative unity value indicates a backward circular motion. A backward elliptic motion is associated with SDI values ranging from –1 to 0 while a forward elliptic motion is associated with SDI values ranging from 0 to 1. When the SDI is null the orbit becomes a straight line. The inclination angle φ of the major axis of the ellipse with respect to the x axis is given by:

$$\varphi = \frac{1}{2} \tan^{-1} \frac{2\,(x_d y_d + x_q y_q)}{x_d^2 + x_q^2 - y_d^2 + y_q^2} \tag{4}$$

In addition to this, the amplitude of the major and minor axes of the elliptical orbit can be evaluated using:

$$a = \sqrt{\frac{2(x_q y_d - x_d y_q)^2}{y_q^2 + y_d^2 + x_q^2 + x_d^2 - \sqrt{\left(y_q^2 + y_d^2 - x_q^2 - x_d^2\right)^2 + 4\left(x_q y_q + x_d y_d\right)^2}}} \tag{5}$$

The shape and directivity index can be defined also as the ratio between the amplitudes of the minor axis and the major axis of the filtered orbit.

Case History

The case history of rotor–to–stator rubs occurred in a large 320 MW turbine–generator unit has been analysed in order to study the effects of this type of fault on the machine vibrations. The rotor train was composed of a high–intermediate–pressure turbine (HP–IP), a low–pressure turbine (LP) and a generator (Figure 1). The three shafts were joined with rigid couplings and were supported on fluid–film journal bearings. The machine running speed was 3000 rpm while the first flexural critical speeds of the HP–IP turbine and the LP turbine were about 1400 rpm and 1150 rpm, respectively. Each bearing was equipped with a couple of *XY* proximity probes and seismic transducers mounted in radial direction 90° apart.

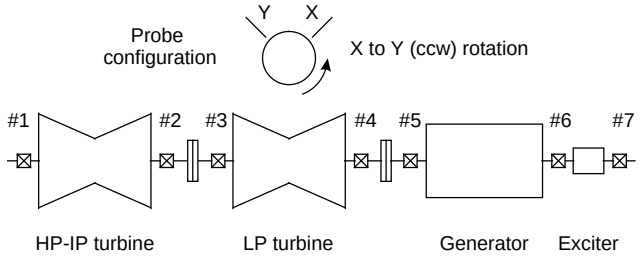

Figure 1. Machine train diagram.

The first speed transient considered, which will be denoted as Case A, is related to the following conditions: at the end of a long scheduled outage the machine was started–up, but the first run-up was aborted just before reaching the operating speed. At first, the speed decreased slowly from 2940 rpm to 1512 rpm. Figure 2 shows the Bode plot of the 1X vibrations measured on bearing #2 during the coast–down in the X and Y directions.

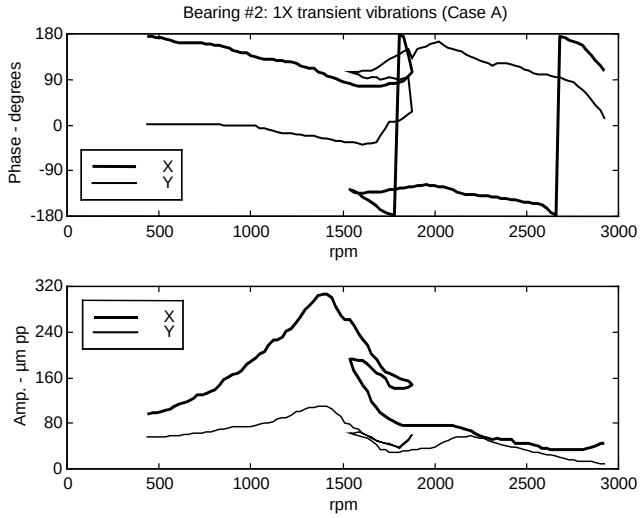

Figure 2. Bode plot of the 1X vibrations measured on bearing #2 during a coast–down (Case A): rub occurrence.

As the first balance resonance of the HP–IP turbine was nearly 1400 rpm, when the speed decreased below 1600 rpm the 1X shaft vibrations at bearings #1 and #2 increased significantly. The control room operators decided to avoid to let the machine pass through the resonance and increased the rotating speed up to 1848 rpm in order to straighten the rotors. However, during this partial run–up the 1X vibrations were quite different from those occurred during the first phase of the run-down. The phase turn was noticeable and also the increase of the vibration levels was considerable. These symptoms were considered the consequences of light rotor–to–seal rubs. Then, it was decided to let the machine slow down passing through the resonance of the HP–IP turbine. In the speed range from 1848 rpm to 1400 rpm the 1X vibrations increased progressively and reached 150 µm pk–pk and 307 µm pk–pk at bearings #1 and #2, respectively. In addition to this, the phase of the 1X vibrations showed an abnormal behaviour (Figure 2). It is possible to presume that while passing through the first critical speed of the HP–IP turbine very high vibrations occurred in the mid–span of the rotor. Likely, this caused further rotor–to–seal rubs. However, the 2X vibrations were low (Figure 3) and showed only small changes in the resonance region that can be ascribed to non–linear effects in the oil–film forces induced by the high 1X vibrations.

When the speed went below the resonance the 1X vibrations decreased progressively but, they were still 97 µm pk–pk at 430 rpm on bearing #2. This can be assumed to be the effect of a the

thermal bow of the rotor induced by the rubs. The symptoms exhibited by the transient vibrations allow one to presume that the contacts between the rotor and the stator were not severe impacts but light rubs. However, the effects of these rubs on the machine dynamic behaviour were considerable. No sub–synchronous or super–synchronous vibration was detected during the coast–down. Moreover, the full spectrum analysis of the shaft vibrations showed that the direction of the vibration precession was forward. A more detailed description of this case history is reported in some previous papers (Bachschmid et al., 2001, Vania et al., 2001).

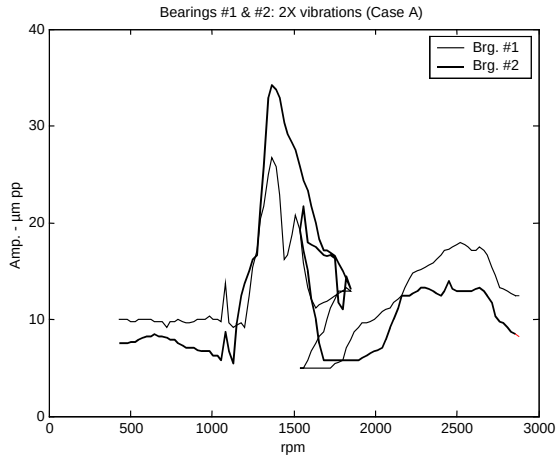

Figure 3. Amplitude of 2X vibrations measured on bearing #1 and #2 in X direction during a coast–down (Case A): rub occurrence.

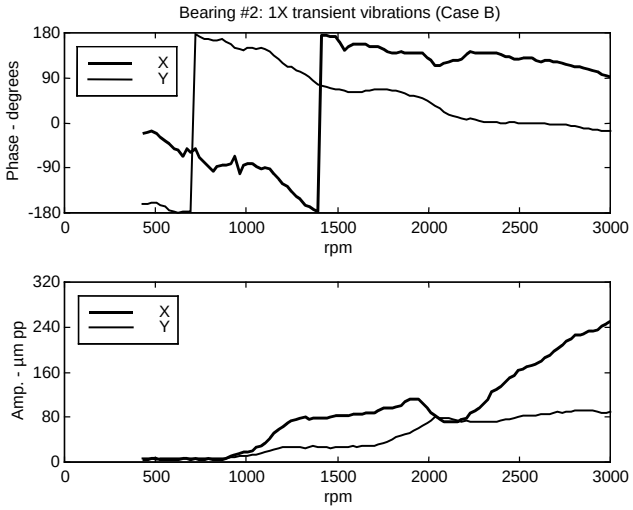

Figure 4. Bode plot of the 1X vibrations measured on bearing #2 during a run–up (Case B): rub occurrence.

Afterward, the machine was rolled for many hours on turning gear in order to straighten the rotors. Fortunately, the shafts did not exhibit any residual bow. In the following days some machine run–ups and run-downs were carried out. Light rotor–to–seal rubs occurred again. These rubbing phenomena always induced only high 1X vibrations and less important 2X vibrations. Figure 4 and Figure 5 show the Bode plots of the 1X vibrations measured on bearing #2, in the X and Y directions, during two run–ups denoted Case B and Case C, respectively. The latter can be considered as a reference run–up since the dynamic behavior occurred during this transient proved to be repetitive. Figure 4 shows that the amplitude of the 1X vibrations increased significantly in the rotating speed range above 2000 rpm and reached 258 µm pk–pk at 3000 rpm. On the basis of a symptom analysis, here not reported for the sake of brevity, this abnormal behavior can be assumed to be the consequence of light rotor–to–seal rubs occurred during the run–up in the rotating speed range near 2000 rpm. It was ascertained during the maintenance that the seal clearances had been adjusted nearly to their lowest acceptable values in order to increase the machine efficiency. This caused the machine dynamic behavior to become critical during the first speed transients when the thermal transient suffered by shafts, casings and foundation is more important.

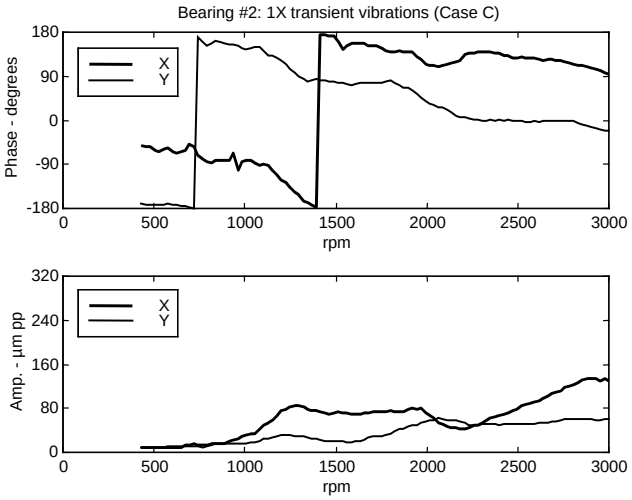

Figure 5. Bode plot of the 1X vibrations measured on bearing #2 during a normal run–up (Case C).

Orbit Shape Analysis

Owing to rotor–to–seal rubs high 1X vibrations occurred on bearing #2 during machine run–ups and coast–downs. In order to investigate the effects of this type of fault on the shape of the 1X orbits, the SDI associated with bearing #2 has been evaluated using the transient vibrations of the Cases A, B and C. Normally the comparison between run–up (like Case B and C) and coast–down (like Case A) transients are not suitable since the machine is respectively in unsteady and steady thermal conditions. Anyhow, as described in the case history, the coast–down of Case A is the consequence of an aborted run–up, therefore the machine was in a similar thermal condition than the two other run–ups.

In order to show the use of the indexes introduced at the beginning of the paper, the speed transient data of Cases A, B and C have been used to evaluate the SDI(Ω) (Figure 6), the amplitude (Figure 7) and the inclination angle (Figure 8) of the major axis of the 1X orbits as functions of the rotating speed.

Owing to the rub occurrence, the SDI(Ω) curve of the 1X filtered orbits (Figure 6) measured during the coast–down (Case A) shows significant differences in comparison with the corresponding curve associated with the reference transient (Case C). The most important differences are in the rotating speed range below 1200 rpm. In fact, as shown by the respective curve of the major axis amplitude of the orbit (Figure 8), during the last part of the machine slow–down, the effects of the shaft bow induced by the rubs were considerable.

During the coast–down A, when the speed decreased below 750 rpm the SDI value dropped below 0.1: that is the orbit became extremely elliptical. This behaviour was abnormal and it was quite different from that one which occurred in the normal transients of the same machine. The SDI(Ω) curves associated (Figure 6) with the run–ups B and C are nearly the same, over the complete speed range

from 600 rpm to 3000 rpm, although the degree of ellipticity of the orbit shows significant changes. In fact, just near 2000 rpm, the 1X orbit at bearing #2 became almost circular, although the major axis amplitude was not very high (Figure 8). At the end of the run–up B, owing to the shaft bow induced by rotor–to–seal rubs, the amplitude of the major axis was significantly higher than that one of the orbits measured at the end of the reference run–up C, during which no rub has occurred. Nevertheless, in the Cases B and C, in the speed range from 2500 rpm to 3000 rpm, the ellipticity of the 1X orbits was nearly the same.

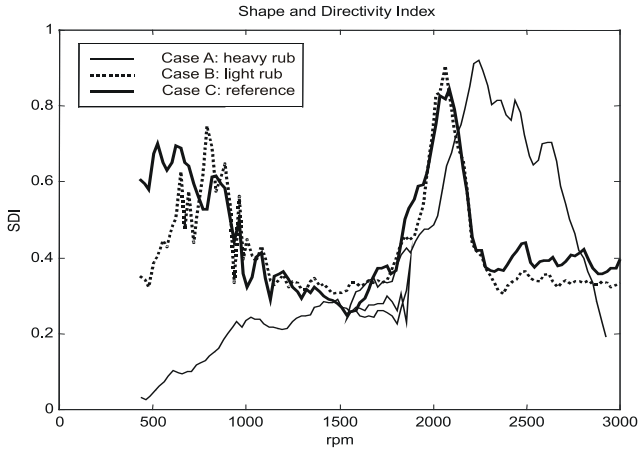

Figure 6. Shape and Directivity Index vs. rotating speed. SDI curves of filtered orbits (1X) evaluated at bearing #2 during the speed transients.

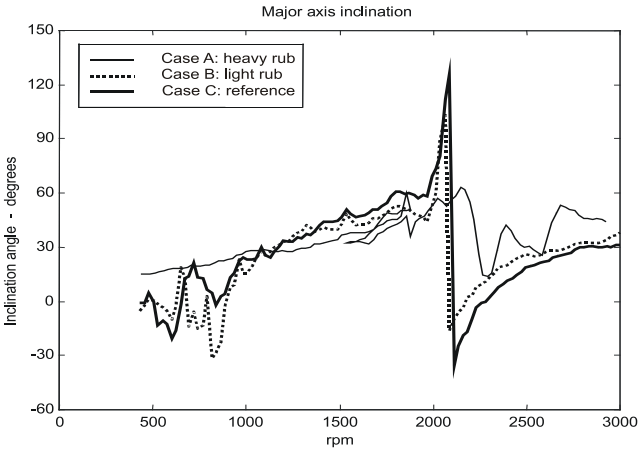

Figure 7. Inclination angle vs. rotating speed. Angular orientation of the major axis of filtered orbits (1X) evaluated at bearing #2 during the speed transients.

Figure 7 shows that the inclination of the major axis of the 1X filtered orbits was not significantly affected by the rubs. However, during the abnormal coast–down A, in the speed range below 800 rpm, that is when the effects of the shaft bow induced by the rubs became important, the values of the major axis inclination differed of nearly 15° from the respective reference values. In addition, during all the transients, significant and fast changes in the major axis inclination occurred in the speed range close to 2000 rpm; in order to explain this fact, it necessary to consider that when the orbit tends to become circular the significance of the inclination angle of the major axis is poor.

Additional information can be obtained by means of Figure 9, which shows the mean value of the oil–film pressure in the bearing #2 measured during the three transients that have been considered. The correlation between abnormal values of the oil–film pressure and the occurrence of large journal orbits has been investigated. During the run–ups B and C, in the rotating speed range below 2000 rpm, the mean pressure of the oil film, as well as the shaft vibrations, showed similar values. Conversely, during the run–up B, when the rotating speed exceeded 2500 rpm, the mean pressure showed higher values in comparison with those of the reference transient (Case C). This behavior is the consequence of the higher amplitude of the 1X filtered orbits.

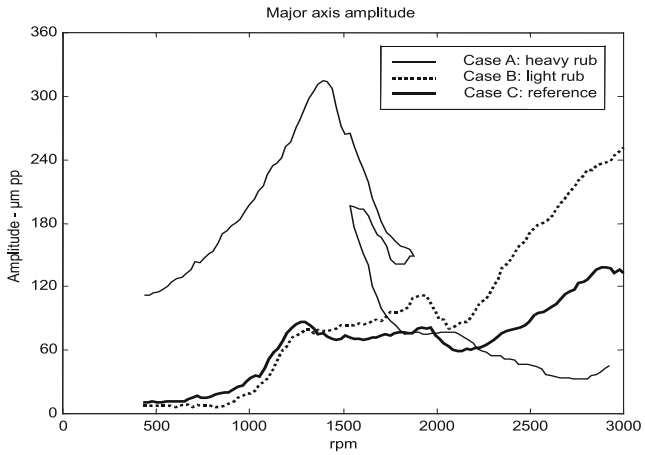

Figure 8. Amplitude of the major axis of the filtered orbits (1X) evaluated at bearing #2 during the speed transients.

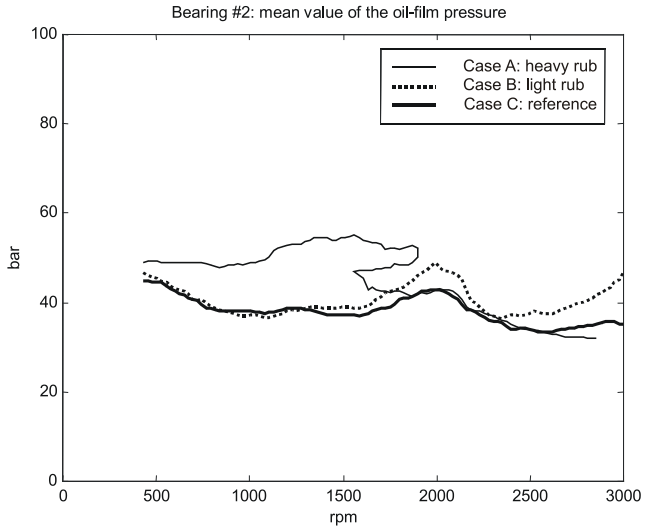

Figure 9. Mean value of the oil–film pressure at bearing #2 during the speed transients.

Figure 4 and Figure 8 show that, owing to the shaft bow induced by the rubs occurred during the run–up B, the synchronous vibrations became very high when approaching the nominal value of the rotating speed. Therefore, it is possible that the significant increase of the journal orbit amplitude caused an increase also of the mean value of the oil–film pressure. An additional contribution to this effect on the oil pressure can be induced by a change in the average position of the journal centre, correlated to the orbit enlargement. However, these phenomena, caused very little changes in the ellipticity and the major axis inclination of the 1X orbit, in comparison with the reference behavior (Figure 6). Therefore, it is possible to presume that also the changes in the dynamic stiffness of the oil–film were unimportant. This low sensitivity of the bearing

stiffness to considerable increases of the journal vibrations can be due also to the presence of a significant oil–film thickness at high rotating speeds.

The curves plotted in Figure 9 show that during the abnormal coast–down (Case A), owing to the effects of the shaft bow induced by the rubs, the mean value of the oil–film pressure measured on bearing #2 increased significantly in comparison with the reference values especially close to 1400 rpm. In the lower range of the rotating speed the minimum height of the oil–film decreases, in accordance with the decrease of the average position of the journal centre inside the bearing. Therefore, when the rotating speed was low, it is possible that the increase of the mean value of the oil–film pressure induced by the large 1X orbit was associated with significant changes in the dynamic stiffness of the bearing. Owing to this, the ellipticity and the major axis inclination of the orbit changed in comparison with the respective reference values (Figure 6 and Figure 7).

Even if the consideration of the oil–film pressure values can give significant diagnostics hints, as shown here, these data are unfortunately seldom available.

The results obtained by means of the analysis of the indexes plotted in Figure 6 to Figure 8 are confirmed by the direct analysis of the orbits at fixed rotating speeds. Figure 10 to Figure 13 show the 1X orbits measured on bearing #2, during the three considered transients, at 2920, 2000, 1400 and 500 rpm, respectively.

Figure 10 confirms that the shaft bow induced by the rubs causes very high synchronous vibrations during the run–up B, as already shown by Figure 8, but the ellipticity of the orbits of the three considered cases is similar, especially that of Cases B and C, as shown by Figure 6.

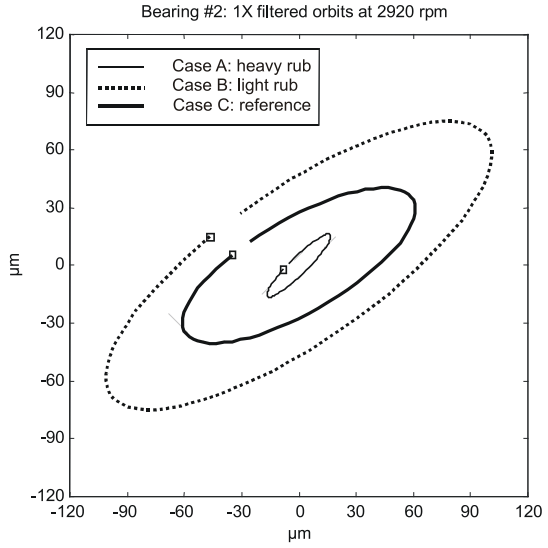

Figure 10. Filtered orbits (1X) measured on bearing #2, at 2920 rpm, during the speed transients (SDI calculated values: Case A, 0.212; Case B, 0.334; Case C, 0.361).

Figure 11 shows that the orbits are very similar in the three cases and close to be circular, explaining in this way the results obtained in Figure 7 about 2000 rpm.

The 1X orbits illustrated at low rotating speed in Figure 13 show that, in the reference case, the major axis was nearly horizontal; conversely, during the abnormal coast–down (Case A) the inclination angle of the major axis of the orbit was nearly 15°. As expected by the consideration about oil–film thickness of Figure 9, also the SDI values of Case A are different from the other speed transients. The occurrence of significant changes in the dynamic stiffness of the oil–film of the bearings should be considered in the model of the fully assembled machine used to simulate the system response and identify the machine faults, otherwise the accuracy of the results could be poor.

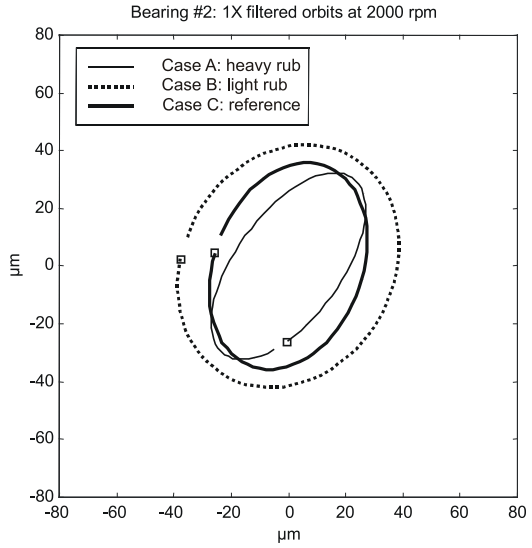

Figure 11. Filtered orbits (1X) measured on bearing #2, at 2000 rpm, during the speed transients.

Figure 12 represents the orbits at 1400 rpm. The differences between the heavy rub Case A and the others two cases is evident and the orbit is very large as shown in Figure 8 and as can be expected by means of the consideration of the oil–film pressure curve of Figure 9.

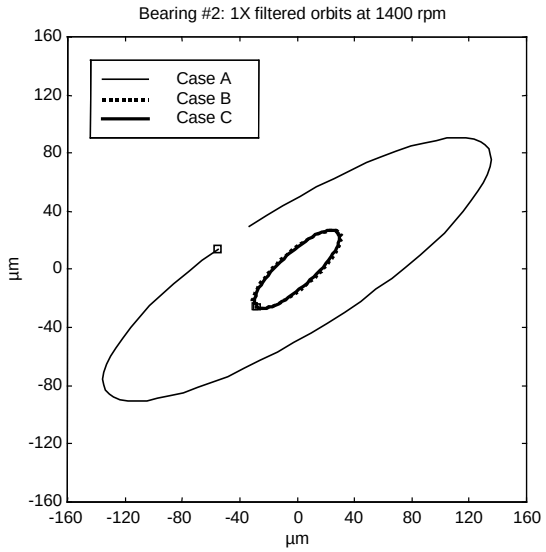

Figure 12. Filtered orbits (1X) measured on bearing #2, at 1400 rpm, during the speed transients (SDI calculated values: Case A, 0.274; Case B, 0.326; Case C, 0.307).

Therefore, the analysis of the SDI(Ω) curve, plotted against the rotating speed of the shaft, provides very useful information that can be used to tune the machine model. In order to obtain more significant information about the journal bearing behaviour the study of the orbit ellipticity can be integrated with the analysis of the changes in the inclination and amplitude of the major axis of the orbit during the machine transients. These indexes, charted as a function of the rotating speed, are able to summarize the consideration that can be made by means of the analysis of several orbit shapes at different rotating speeds.

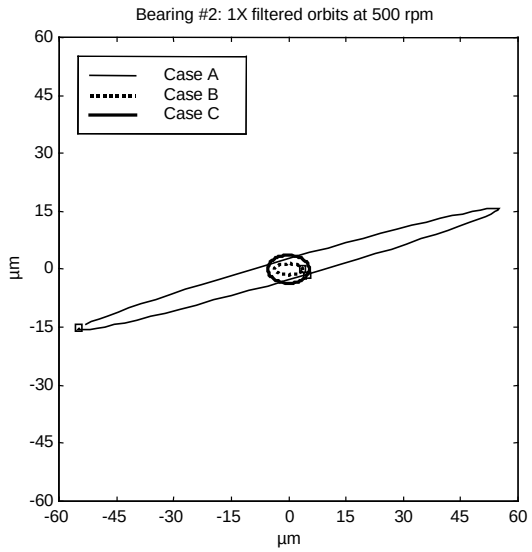

Figure 13. Filtered orbits (1X) measured on bearing #2, at 500 rpm, during the speed transients (SDI calculated values: Case A, 0.048; Case B, 0.391; Case C, 0.702).

Model-based Identification of the Fault

Some techniques can be used to identify the severity and the location of the machine fault. In the past, the authors have carried out a first identification of the rotor–to–seal rub occurred in the Case A using a model–based method developed in the frequency domain (Bachschmid et al., 2000, Bachschmid et al., 2002). Some results of this investigation have been published in a previous paper (Vania et al., 2001). Finite Elements (FE) are used to model the machine rotor train, while rotating speed dependent coefficients are used to model the dynamic stiffness of the journal bearings. In addition, different techniques can be used to model the machine foundation. In the end, the most important types of fault can be modelled with suitable sets of exciting forces and moments that can be applied to the nodes of the FE model of the rotors. The amplitude, the phase and the location of the exciting forces are estimated by minimising the error between the experimental transient vibrations and the respective numerical response provided by the model of the rotor system. A detailed description of this fault identification method is shown in a previous papers (Bachschmid et al., 2002). The relative error, ε, between experimental data and numerical results can be expressed in the form:

$$\varepsilon = \sqrt{\frac{(\mathbf{X}_{th}^{*} - \mathbf{X}_{exp}^{*})^{T} (\mathbf{X}_{th} - \mathbf{X}_{exp})}{(\mathbf{X}_{exp}^{*T} \cdot \mathbf{X}_{exp})}} \qquad (6)$$

where $*$ indicates complex conjugation, $\mathbf{X}_{exp}$ is the vector of the experimental vibrations evaluated at the degrees of freedom that have been selected for the identification process, while $\mathbf{X}_{th}$ is the corresponding vector of the theoretical response obtained with the model. Usually, this relative error ε is called residual.

In the considered case, the model of the rotor train is shown in Figure 14. This model is composed by 122 beam elements.

The three shafts of the machine train, connected by rigid couplings, were supported on seven elliptical oil-film journal bearings. The ratio between the radial clearance of the bearings and the radius of the respective journal ranged from 0.0017 to 0.0026.

The dynamic stiffness of the oil-film journal bearings have been evaluated by integrating the Reynolds equation.

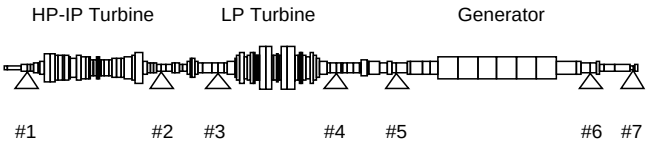

Figure 14. Rotor train model.

The seals of the steam turbines have not been included in the model used to identify the machine fault. This inaccuracy of the model does not affect significantly the accuracy of the investigation as the system response due to the rotor-to-stator rubs is not simulated in the time domain by taking into account of the actual evolution of the contacts between the shaft and the seals. Conversely, the aim of this study is to identify the equivalent bending moments that allow the shaft bow induced by the friction forces caused by the rubs to be simulated in the frequency domain. Therefore, the machine model must be adequate to fit the trend of the experimental 1X vibrations induced by the shaft bow. The magnitude on the identified equivalent bending moments will take into account of the effects due to the additional stiffness caused by the temporary contacts between the shaft and the seals. Moreover, it is necessary to consider that in this case the seals were linked to flexible mountings and the fluid that flowed through the seals was compressible: owing to this the additional radial stiffness of the shaft induced by the contacts is less important with respect to the occurrences of heavy rubs in other types of rotating machines such as pumps.

The rubs occurred during the machine coast–down (Case A) caused changes mainly in the synchronous vibrations of the shafts. These vibrations were due to a shaft thermal bow of the HP–IP turbine that was induced by the friction forces occurred during the rotor–to–seal rubs. Therefore, the local bow of the shaft has been modelled by applying a couple of equal but opposite bending moments to the ends of a short length of the shaft. In order to identify the fault, the 1X transient vibrations induced only by the rubs have been analysed. These additional vibrations have been estimated by subtracting the 1X vibration vectors measured during the reference transient (Case C) from the respective 1X vectors measured during the abnormal coast–down (Case A). This approach assumes that the behavior of the system is linear. Owing to the development of the rubs the shaft bow severity changed during the coast–down. Therefore, the amplitude of the equivalent bending moments depended on the time and the rotating speed, as well (Figure 15). Good results had been obtained with a first attempt to identify the location and the severity of the rubs.

However, on the basis of the results of a more recent analysis of the ellipticity index and the major axis inclination of the journal orbits occurred during the coast–down, it has been decided to carry out a further fault identification using a refined machine model, using the results of the previous paragraph. In particular, the stiffness coefficients of bearings #1 and #2 have been slightly modified in the rotating speed range from 400 rpm to 1000 rpm.

In fact, using the original bearing coefficients, at a rotating speed of 500 rpm, the bending moments that had been identified in the past caused a 1X orbit on bearing #2 whose major axis was almost horizontal. This results is not completely in accordance with the experimental data (Figure 13). Then, the direct stiffness coefficients in vertical and horizontal direction have been changed of 40% and 15% respectively. The two cross–sections where the bending moments have been identified (Figure 16) are near the mid–span of the rotor: in this zone some labyrinth seals separate the HP turbine from the IP turbine. The residual, ε, evaluated by considering the shaft vibrations associated with eight rotating speeds spaced in the range from 500 rpm to 1800 rpm was 0.4289.

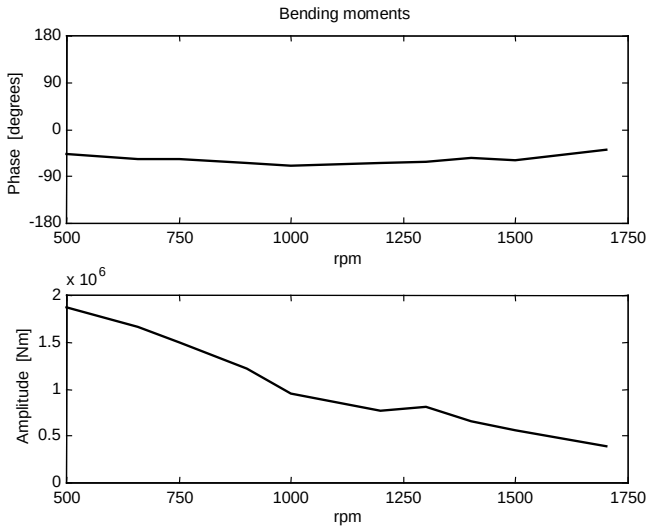

Figure 15. Amplitude and phase of the identified bending moments vs. rotating speed.

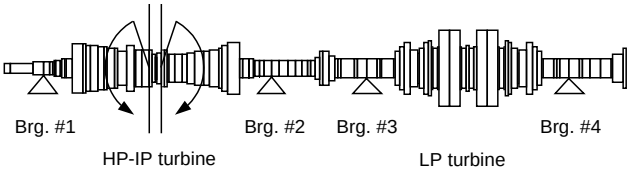

Figure 16. Axial position of the identified bending moments.

If the previous mis–tuned model is used, the residual increases to 0.5004. The journal orbits (1X) at bearing #2, obtained with the refined model by considering the identified bending moments, have been analyzed and compared with the respective orbits evaluated using the experimental additional vibrations caused by the rubs. Figure 17 shows the comparison between the curves of the SDI(Ω) obtained using experimental data and numerical results. The accordance between these two curves is rather good over the complete range of the rotating speed that has been analyzed. In addition to this, Figure 18 shows the comparison between the curves of the inclination of the major axis of the orbit evaluated on the basis of experimental data and numerical results. Also the accordance between these curves is satisfactory. In the end, in Figure 20, the experimental additional transient vibrations induced by the rubs during the costdown (Case A) are compared to the 1X vibrations evaluated at bearing #2 with the simulating model. Also in this case the model–based diagnostic technique has provided successful results.

In order to emphasize the increase of accuracy of the fault identification obtained by refining the original machine model, some results provided by a further analysis are shown. Figure 21 shows the journal orbits evaluated at 500 rpm, on bearing #2, using the tuned and the mis–tuned stiffness coefficients (Case studies n.2 and n.3). These two orbits, evaluated using the same bending moments, are compared with the respective 1X filtered orbit evaluated by considering the experimental additional vibrations of the shaft (Case n.1).

The accordance between the experimental orbit and that one evaluated using the tuned model is very good, although the ellipticity of the orbit is considerable. On the contrary, the journal orbit induced by the same bending moments, but evaluated with the mis–tuned model, shows a greater ellipticity and its major axis is almost horizontal, just like the experimental orbit occurred in the reference transient C: that is in absence of rubs (Figure 13). This different behavior of the simulated orbits is caused only by the changes that have been made in the stiffness coefficients of bearings #1 and #2. The effects of the use of the mis–tuned model on the journal orbit is evident, however, the errors in the simulation of the shaft vibrations are still more important. Owing to this, in the lower range of the rotating speed, the accuracy of the previous fault identification decreased significantly. In fact, using the tuned model, the residual ε evaluated by considering the shaft vibrations associated with rotating speed of 500 rpm only, was 0.4939.

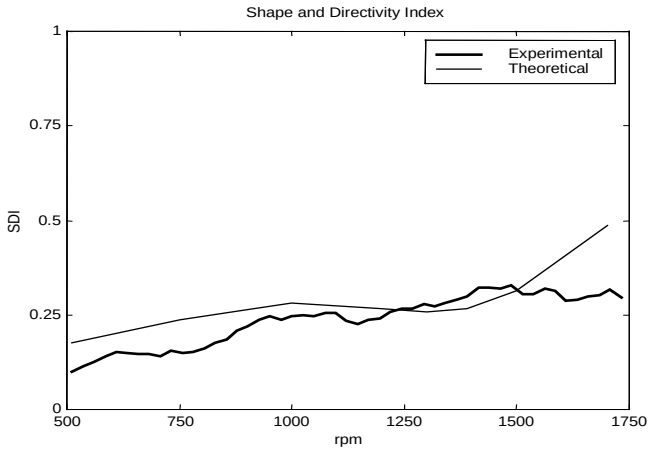

Figure 17. Shape and Directivity Index vs. rotating speed : comparison between experimental data and numerical results.

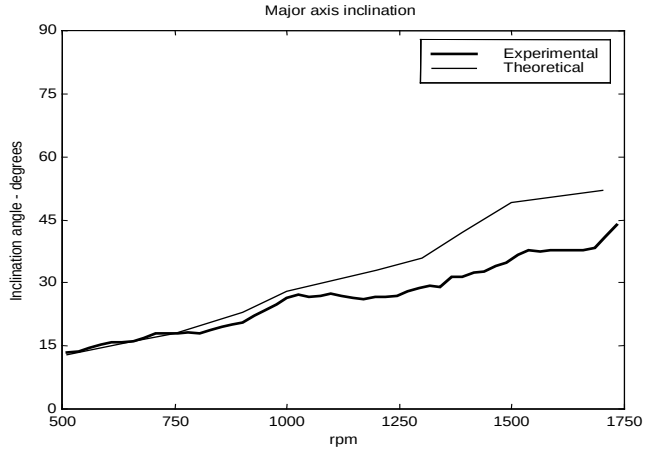

Figure 18. Major axis inclination vs. rotating speed: comparison between experimental data and numerical results.

Conversely, if the mis–tuned model is used, the residual increases to 0.5486. In the end, the identified bending moments have been substituted with an unbalance located in the mid–span of the axial position of the two moments. Then, the mis–tuned model of the machine has been considered to simulate the machine response at 500 rpm. A suitable magnitude of the unbalance has been evaluated in order to cause a journal orbit, at bearing #2, whose major axis had the same amplitude of the orbit caused by the identified bending moments (Case n.3). The journal orbit induced by this unbalance is shown in Figure 21 (Case n.4). The ellipticity and the orientation of this orbit are very similar to those of the orbit, evaluated with the same model, but caused by the bending moments. Therefore, for this case study, the shape and the orientation of the orbit are not affected by the type of the excitation. Anyhow, in this investigation, the two opposite bending moments and the unbalance were applied, separately, in the same portion of the shaft. Then, the

difference between the inclination of the experimental orbits and the inclination of the major axis of the orbits simulated with the model can be just ascribed to the effects of inaccurate estimates of the bearing coefficients.

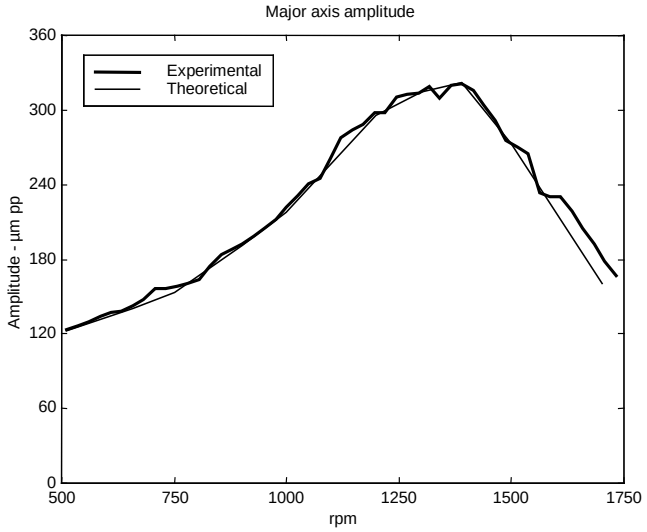

Figure 19. Amplitude of the major axis of the 1X filtered orbit vs. rotating speed: comparison between experimental data and numerical results.

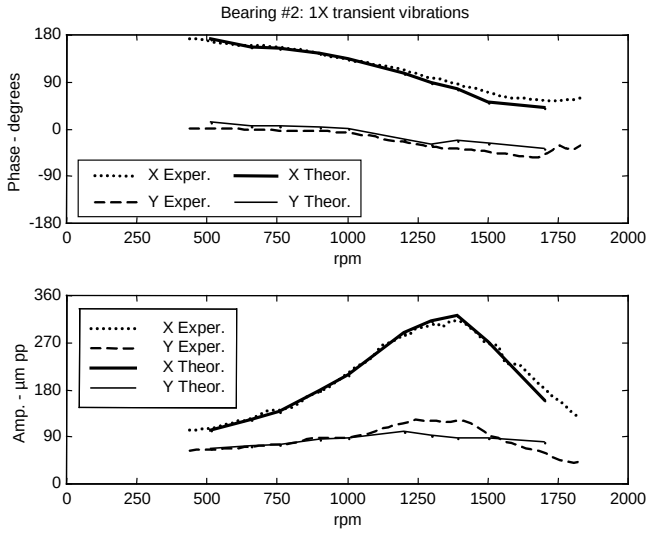

Figure 20. Bode plot of the 1X additional vibrations on bearing #2 induced by the rubs: comparison between experimental data and numerical results.

Conclusions

In the investigation described in this paper, the results of the full spectrum analysis of rotating machine vibrations have been considered. In particular, the analysis of the changes in the Shape and Directivity Index, inclination and amplitude of the orbit major axis that occur during run–ups and coast–downs, has proved to enable very useful diagnostic information to be obtained. In fact, abnormal changes in the ellipticity of the orbit and the direction of the vibration precession are significant symptoms of some types of fault. In addition, the results of the SDI analysis, of the amplitude and the inclination of the major axis of the orbit during the machine speed transients can be used to tune the bearing coefficients that are included in the machine model. An example of a real machine model tuning and of the improvement obtained in the fault identification procedure is presented at the end of the paper.

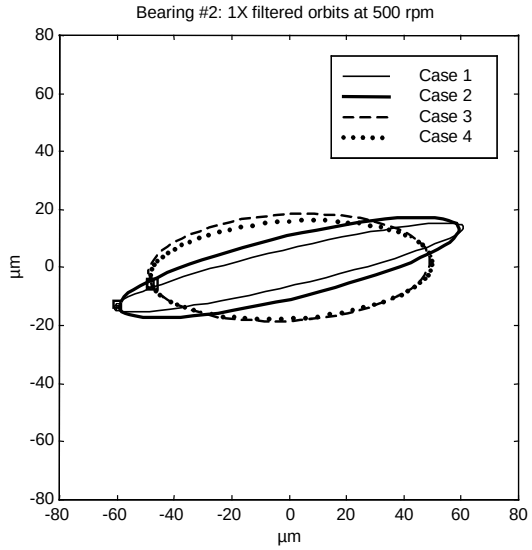

Figure 21. Filtered orbits (1X) on bearing #2 evaluated at 500 rpm. Case 1: experimental orbit. Case 2: data simulated with the identified bending moments and the tuned bearing stiffness. Case 3: data simulated with the identified bending moments and the mis–tuned bearing stiffness. Case 4: data simulated with an unbalance and mis–tuned bearing stiffness.

References

Bachschmid N., Pennacchi P., Tanzi E. and Vania A., 2000, "Accuracy of Modelling and Identification of Malfunctions in Rotor Systems: Experimental Results", Journal of the Brazilian Society of Mechanical Sciences, Vol. XXII, No 3, pp. 423-442.

Bachschmid, N., Pennacchi, P. and Vania, A., 2001, "Spiral Vibrations Due to a Rub: Numerical Analysis and Field Experiences", Schwingungen in Rotierenden Machinen V, SIRM 2001, Wien, pp. 87–96.

Bachschmid, N., Pennacchi, P. and Vania, A., 2002, "Identification of Multiple Faults in Rotor Systems", Journal of Sound and Vibration, 254(2): pp. 327–366.

Lee, C.W. and Joh, C.Y., 1994, "Use of Directional Spectra for Diagnosis of Asymmetry/Anisotropy in Rotor Systems", 4th Int. Conference on Rotor Dynamics, Chicago, USA, Sep. 1994, pp. 97-101.

Lee, C.W., Park, J.P., and Han, Y.S., 1997a, "Use of Directional Spectra for Detection of Misfired Engine Cylinder", Shock and Vibration, Vol. 4, No. 5, 6, pp. 391-401.

Lee, C.W., Han, Y.S., and Lee, Y.S., 1997b, "Use of Directional Spectra of Vibration Signals for Diagnosis of Misalignment in Rotating Machinery", 5th Int. Congress on Sound and Vibration, Adelaide, Australia, Vol. 2, pp. 997-984.

Lee, C.W. and Han, Y.S., 1999, "Directional Time–Frequency signal Processing Techniques for Transient Rotating Machine Vibration Analysis", *IFToMM '99 Proceedings of the 10th World Congress of the Theory of Machines & Mechanisms*, Oulu, Finland, pp 1692–1697.

Lee, C.W. and Han, Y.S., 1998, "Directional Wigner Distribution and its Applications", Journal of Sound and Vibration, Vol. 216, No. 4, pp. 585-600.

Soutwick, D., 1993, "Using full Spectrum Plots – Part 1", Orbit, Vol. 14, No. 4, Bently-Nevada Corporation, pp. 19-21.

Soutwick, D., 1994, "Using full Spectrum Plots – Part 2", Orbit, Vol. 15, No. 2, Bently-Nevada Corporation.

Vania, A., Bachschmid, N. and Pennacchi, P., 2001, "Analysis of Light Rotor–to–Stator Contacts in Large Turbine–Generator Units", 4th Int. Conference on Acoustical and Vibratory Surveillance Methods and Advanced Diagnostic Techniques, Compiègne (France), pp. 507–516.